Arabian Journal for Science and Engineering (2023) 48:8769–8783
https://doi.org/10.1007/s13369-022-07419-8

RESEARCH ARTICLE-CHEMICAL ENGINEERING

Influence of Nano-glass Powder on the Characteristics Properties as Well as Stability Against Firing for Geopolymer Composites

H. M. Khater[1] · **M. Ghareeb**[1]

Received: 26 March 2022 / Accepted: 23 October 2022 / Published online: 10 November 2022

Abstract
Influence of nano-glass powder on physico-mechanical properties of geopolymer composite materials has been studied, in addition to studying their firing stability against high temperature from 500 up to 1000 °C. For increasing mechanical, physical as well as firing stability for metakaolin composites; Nano-glass powder was used. Alumino-silicate materials are kaolin, fired kaolin (metakaolin) and limestone all pass 75 μm. Materials prepared at water/binder ratios in a range of 0.40; whereas the used activator 5 M sodium hydroxide with equal volume of liquid sodium silicate. Nano-glass powder added as a partial replacement for metakaolin material in the ratio of 1 up to 9%. Results indicated that compressive strengths of geopolymer mixes incorporating Nano glass powder were obviously higher than those of control one and increased up to 7% followed by slight decrease of on using 9%. Firing of hardened geopolymer results in high thermal resistance up to 500 °C then exposed to decrease up to 800 then increased again at 1000 °C for specimens incorporated 7 and 9% nano-glass powder. However, no micro-cracks were noticed up to 800 °C for all samples as recorded by visual examination of the fired samples.

Keywords Nano-glass · Geopolymer composites · Thermal stability · Firing

1 Introduction

Since a very long time ago, nanotechnology has existed as both a science and a technology. It is more of a development of long-standing sciences and technology and represents a smaller-scale continuation of inquiry into the nature of our world. The aforementioned Nano-scale technologies will have an impact on virtually every part of the construction process.

When compared to traditional grain-size materials of the same chemical composition, nanoscale particle size can result in dramatically better characteristics. According to Balaguru and Chong [1], nanomaterials have distinctive physical and chemical properties that can help create materials that are more effective than those that are now available. Nanoparticles have advantageous properties due to their exceedingly small size. Furthermore, the rapid advancement of nanoscale materials science has provided civil engineers with a new window of understanding into traditional construction materials such as cementitious materials and steel, allowing us to improve their properties, extend their lifetime, and save money and energy [2].

Khater et al. [3], investigated the effect of Nano silica in a range of concentrations from 0 to 1.5% on alkali-activated slag geopolymer. When compared to the control mix after 90 days, the results demonstrated that increasing the amount of Nano silica improves mechanical properties. Experimental and mathematical evaluations are used to examine thermal properties for various ratios. The study discovered that increasing the ratio of Nano silica improves thermal characteristics and thermal insulation. Kuo et al. demonstrated that SiO_2 and Fe_2O_3 nanoparticles improved the compressive and flexural strengths of cement mortars [4].

Due to their high activity, it has been demonstrated that nanoparticles that are uniformly scattered in a cement paste will expedite cement hydration [5]. Additionally, the nanoparticles will fill cement pores, improving the cement's microstructure and the contact between the cement paste and aggregates in concrete as well as its strength. It was also shown that nano-Fe_2O_3 has the ability to self-sense strain, which could be valuable for structural health monitoring [6, 7].

✉ H. M. Khater
hkhater4@yahoo.com

[1] Housing and Building National Research Centre (HBNRC), 87 El-Tahrir St., Dokki, Giza, P.O. Box 1770, Cairo, Egypt

Table 1 Chemical composition of starting materials (Mass, %)

Oxide content (%)	SiO_2	Al_2O_3	Fe_2O_3	CaO	MgO	SO_3	K_2O	Na_2O	TiO_2	MnO	P_2O_5	Cl^-	SrO	BaO	L.O.I	Total
Kaolin (M. East)	49.86	34.10	0.30	0.09	0.26	0.59	0.02	0.03	0.88	0.00	0.35	0.00	0.00	0.00	13.44	99.92
Kaolin south sinal	50.10	31.46	1.42	0.31	0.19	0.14	0.08	0.12	2.67		0.14	0.07	0.00	0.00	13.01	99.81
MK (fired kaolin at 800° for 2 h)	62.37	31.60	1.47	0.26	0.01	0.01	0.15	0.12	2.60	0.00	0.01	0.03	0.01	0.00	1.16	99.86
Lime stone	0.52	0.18	0.04	55.86	0.15	0.20	0.01	0.22	0.00	0.00	0.12	0.06	0.00	0.00	42.60	99.96
Nano-glass powder	70.25	0.88	0.21	11.90	3.42	0.41	0.09	9.99	0.06	0.00	0.01	0.09	0.01	0.00	2.63	99.95

Through measurements of physicomechanical and morphological parameters of hardened specimens, Khater [8] investigated the effect of Nano-SiO_2 (NS) addition on attributes of Geopolymer materials. Nano-silica was added to the total weight in increments of 0.5%, ranging from 0 to 3%. In addition, using albite instead of slag creates a light binder with promising mechanical properties. The compressive strengths of Geopolymer mixes incorporating NS were clearly higher than those of control mixes, especially at young ages and up to 2.5% NS with the lowest percentage of water absorption. Khater and Abd el Gawwad [9] also demonstrated the impact of nano-kaolin on the alkaline activation of slag-metakaolin (AAs) binder for the creation of environmentally acceptable geopolymer materials (40:60 wt.%), of geopolymer binder. Results demonstrate enhancement in both mechanical and microstructural characteristics with Nano-kaolin up to 5%, while further increase resulted in agglomeration and strength decrease.

The size-related properties of nanoparticles may differ from those of bulk materials. They show how bulk materials and molecular structures are connected. At the nanoscale, the percentage of atoms on a material's surface becomes significant, resulting in unique properties, such as gold nanoparticles melting at 300 °C versus gold slabs melting at 1064 °C [10, 11].

When nanoparticles (typically SiO_2, TiO_2, etc.) are added to cement-based materials, a series of chemical bond connections between the nanoparticles and cement hydration products are formed, and the nanoparticles may become the crystal nucleus of the calcium silicate hydrate (C-S-H) gel, in addition to working as nano filler. They fill the holes between the cement grains to densify the microstructure of the cement paste. The entire system will then transform into a dense network structure with nano-particles as the cores, thereby refining the microstructure of cement-based materials [12–19].

However, the complicated manufacturing method and expensive cost of these nano-particles prevent their widespread use in cement-based materials. As a result, novel nano-particles as an alternative to traditional nano materials with excellent performance, cheap cost, and a simple manufacturing process are critical for the construction industry's long-term growth. To create a new nano-metric SCM, micrometric waste glass powder with a high amorphous silica content (70–80 wt.%) is vaporized and nucleated into spheroidized glass powder (SGP) using an induction thermal plasma torch, a method similar to silica fume synthesis (SF). The capacity of this method to evaporate and nucleate waste glass into glass nanoparticles has already been proven [20].

SGP was compared to finely ball-mill ground glass powder (GP) and SF in terms of their reactivity in cement pastes and mortars. When SGP, GP, and SF are used as a partial replacement for OPC in cement pastes and mortars, this paper discusses the characterization of the materials used as well as the results of reactivity, polymerization of the C-S-H chain, and compressive strength development. The main goal of this paper is to investigate the effect of Nano-glass powder addition on the physico-mechanical properties of the resulting geopolymer materials made from various aluminosilicate precursors, in order to develop nontraditional cementing materials with a high potential for use in high-temperature environments, where the hardened mixes' thermal stability will be tested. Testing of the resulting geopolymer product is

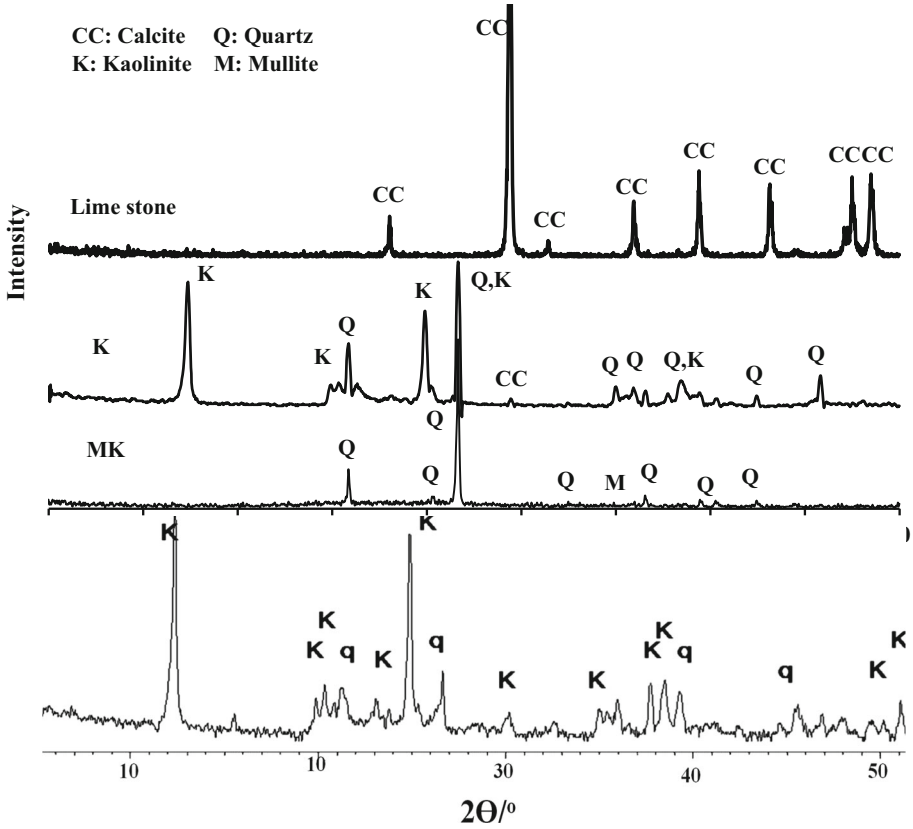

Fig. 1 X-ray diffraction pattern of used raw materials

studied by X-ray diffraction (XRD), FTIR, DTG, compressive strength testing, as well as visual examination of the fired samples are conducted on pastes of Geopolymer based sample, in order to generate a better understanding of the effect of the Nano-glass on the behavior of Geopolymerization reaction as well as their stability against high temperature.

2 Experimental Procedures

2.1 Materials

High-purity kaolinite material purchased from Middle East Company, Egypt, and kaolin obtained from El-Dehesa, South Sinai, Egypt, as well as powder limestone, was employed in this study. SHIDO Co., Egypt, provided sodium hydroxide (NaOH) pellets with a purity of 99%, which were utilised as alkali activators. Additionally, commercial sodium silicate was employed as an activator. Table 1 shows the chemical compositions of the beginning raw components (1). The raw materials were characterised mineralogically by X-ray diffraction analysis in powder form, as shown in Fig. 1.

The mineralogical composition of the kaolinite material, on the other hand, revealed that it is primarily composed of kaolinite minerals with minor amounts of quartz minerals, as shown in Fig. 1. The chemical composition of the kaolinite material, on the other hand, revealed that it is composed of about 50% silica oxide and 31.5% alumina oxide, with minor content of calcium and magnesium oxides. To make metakaolin, this kaolinite material was thermally processed at 800 °C for 2 h at a rate of 5 °C/min (Mk). This temperature was chosen based on previous research findings that calcinations below 700 °C result in a less reactive metakaolinite with more residual kaolinite, whereas calcinations beyond 850 °C crystallize and reactivity declines [21–24].

The nano-glass powder utilized in this study is a synthetic product with spherical particles ranging in size from 35 to 125 nanometers that were created by dry grinding glass powder for 8 hours. The chemical investigation revealed that the principal components are silica and alumina. Table 1 lists the physical parameters of nano-glass powder (2). According to the laser particle size distribution pattern of nano-silica, the average particle size of Ng's crystals is 60 nm.

To examine the particle size of the employed nano-glass powders, a transmission electronic microscope (TEM) of type JEOL-JEM-1230 with magnification up to 60,000 was used. Figure 2 depicts the morphologies of NG particles, which are represented as strongly agglomerated clusters of varying sizes (40–65 nm).

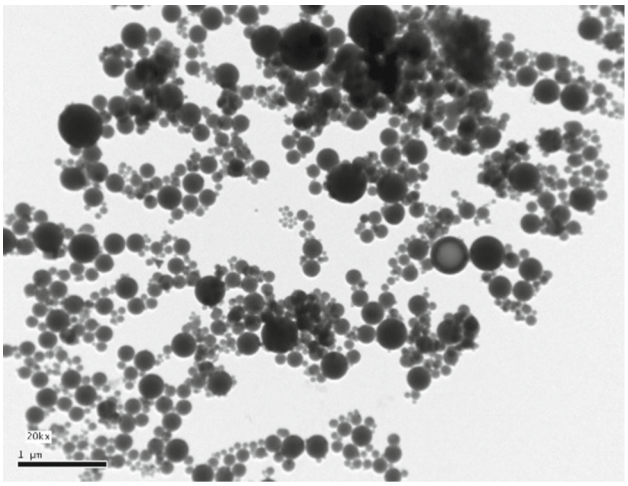

Fig. 2 TEM of the used nano-glass waste powder

2.2 Dispersion of Nano Glass Powder

The nano glass powder was first sonicated for 15 min with a Fritish 450 Sonifier Analog Cell Distributor [25]. Glenium Ace 30-polycarboxylate-based superplasticizer is utilised for Nano-glass powder dispersion since it has been shown to be effective for Nano-glass dispersion [26]. To determine the threshold ratio of the employed Nano-materials, nano-glass was added in the ratios of 0, 1, 3, 5, 7, and 9% of the total weight.

2.3 Composite Preparation and Curing Regime

Because of their high surface energy, nanoparticles are difficult to spread uniformly. As a result, mixing was done as follows:

1. A high-speed magnetic stirrer was used to stir nano-glass powder with 50% of the mixing water for 15 min.
2. After being manually mixed with the alkaline activator solution and the other half of the mixing water for 10 min, the geopolymer materials that had passed through a sieve of 90 m, as shown in Table 2, were rotary mixed for an additional 5 min at medium speed (80 rpm) for an additional 30 s.
3. The previously agitated Nano-silica was added, then the Glenium Ace-30 superplasticizer (polycarboxylate based) was added and spun for an additional 30 s.
4. Allow 90 s for the mixture to rest before mixing for 1 min at high speed.

The addition of 5 M NaOH to dry mixes, as well as 20% sodium silicate to the dry mix, was used in all of the studies. The water-binder material ratio (w/b) rises as the nano content rises, as seen in Table 2.

Table 2 Composition of the geoplymer mixes (Mass, %)

Mix	Kaolin M.E. (%)	MK (%)	Lime stone (%)	Nano-glass (%)	NaOH (5 M) (%)	Na_2SiO_3 (%)	SP (%)	T.water/binder	Total M_2O/Al_2O_3	SiO_2/Al_2O_3	$SiO_2/(Al_2O_3{}^+ M2O)$	Total M_2O/SiO_2
NG0	25	50	25	0	20	20	1	0.40	0.66	2.06	2.11	0.19
NG1	25	49	25	1	20	20	1	0.40	0.67	2.09	2.12	0.19
NG3	25	47	25	3	20	20	1.2	0.40	0.71	2.15	2.14	0.19
NG5	25	45	25	5	20	20	1.4	0.40	0.74	2.22	2.16	0.20
NG7	25	43	25	7	20	20	1.6	0.40	0.78	2.28	2.18	0.20
NG9	25	41	25	9	20	20	1.8	0.40	0.82	2.36	2.21	0.20

The paste mixture was poured into 25 25 25 mm cubic-shaped moulds, vibrated for compaction, and covered with a lid to minimize evaporable water loss.

Specimens were permitted to cure undisturbed for 24 h at room temperature (23 °C), then demolded and some left to be water cured at room temperature.

The specimens were withdrawn from their curing condition at the end of the curing regime, dried thoroughly at 80 °C for 24 h, and then subjected to compressive strength measurements, while the other values were calculated using the crushed specimens that were obtained. After 28 days, samples were paused for hydration by drying at 105 °C for 24 h, and then exposed to firing from 500 up to 1000 °C for 2 h with a heating rate of 5 °C/min.

2.4 Methods of Investigation

Axios (PW4400) WD-XRF Sequential Spectrometer was used for chemical analysis (Panalytical, Netherland). Compressive strength tests were performed on a five-ton German Brüf pressing machine at a loading rate of 100 kg/min, as specified by ASTM C109 M [27]. A Cu-Kα source with a post sample Kα filter was used for XRD analysis using a Philips PW 1050/70 Diffractometer. From 0° to 50° 2θ (step size 0.02° 2θ and speed 0.4° θ/min), XRD patterns were obtained. As an internal standard, silica was used. The XRD software was used to identify the data (pdf-2: database on CD-Release 2005).

A laser scattering particle size distribution analyzer was used for particle size analysis (Horiba LA-950, Kyoto, Japan). For preventing additional hydration, crushed specimens were subjected to a stopping alcohol/acetone solution (1:1), followed by acetone washing, as advised by other investigators [28, 29].

Bulk density was calculated using the formulae [30, 31]:

$$\text{Bulk Density} = D/(W - S)\ (\text{g/cm}^3).$$

where D, weight of specimen; S, weight of suspended specimen in water; and W, weight of soaked specimen suspended in air.

Strength change factor of the hardened samples was calculated according to the following equation [32, 33]:

$$\text{SCF} = 100 * (F_i - F_f)/F_i$$

where F_i is the 28 days compressive strength of the unfired sample, while F_f is the compressive strength of the fired sample at the specified temperature.

The particle size of the nano was measured using a Transmission Electronic Microscopic (TEM) (type JEOL-JEM-1230) with magnification up to 60,000. A Jasco-6100 Fourier transformed infrared spectrometer FTIR was used to examine the bonding characteristics of the alkali-activated specimens. At a weight ratio of KBr: specimen = 200:1, the test sample was pulverized and uniformly mixed with KBr. The 0.20 g mixture was squashed into a 13 mm diameter disc for examination at 8 t/cm^2. The wave number varied between 400 and 4000 cm^{-1} [34, 35].

3 Results and Discussion

3.1 Nano-glass Effect on Geopolymer Composite Properties

FTIR spectra of 28 days hardened geopolymer specimens having various Ng- powder are shown in Fig. 3. The addition of kaolinite up to 7% nano-glass powder causes continuous dissolution and polymerization, which results in the formation of additional binding geopolymer constituents and a decrease in the kaolinite peaks above 3600 cm^{-1}. This increased matrix reinforcement is supported by an increased intensity of the asymmetric stretching vibration (Ti–O–Si) at about 1000 cm^{-1} where T = Si or Al, as resulted of the increased geopolymerization and precipitation. Also, there is a slight shift of the previous band to lower wave number with Nano-glass increase up to 7% reflecting an increased vitreous content within the matrix. This is accompanied by a small rise in the intensity of the symmetric stretching vibrations (Al–O–Si) at around 780 cm^{-1} and the symmetric stretching vibrations (Si–O–Si) at roughly 670–690 cm^{-1}.

Also, regions close to 460 cm^{-1} attributed to angular deformations of SiO_4 tetrahedrons (O–Si–O), as well as asymmetric stretching vibration for Si–O–Si (for non-solubilized particles) probably associated with quartz [36], these results are similar to those obtained by Palomo et al. [37]. Stretching vibration for Al–OH at about 916 cm^{-1} resulted from free unreacted aluminum species from added kaolinite decreased also with time as unreacted free alumina exposed to dissolution and polymerization with time [34].

FTIR spectra of alkali-activated paste enhanced with 7% Ng powder at various hydration ages up to 28 days (Fig. 4), shows the formation and the growth of broad asymmetric T–O–Si band for three-dimensional geopolymer network (N-A-S-H gel) at about 1000 cm^{-1}, which exposed to an increased intensity up to 28 days. This increase reflects the growth in amorphous geopolymer structure as related to the increased dissolution of aluminosilicate precursors with time.

Also, this reflects an enhancement for geopolymerization reaction as well as offering more nucleation sites for geopolymer gel growth and accumulation [38]. The previous elucidation coincides with the decreased intensity of shoulder at about 1100 cm^{-1} for non-solubilized silica as well as a decrease in kaolinite peaks beyond 3600 cm^{-1} with time.

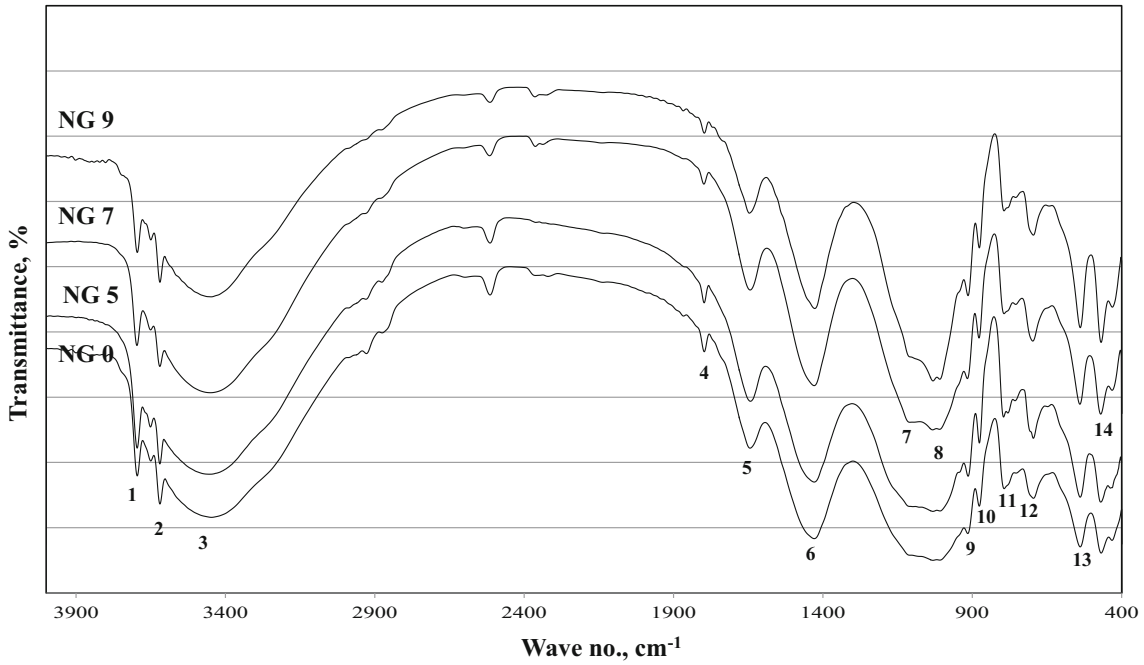

Fig. 3 FTIR spectra of 28 days alkali activated specimens enhanced with various ratios of nanoglass. [1, 2, 3: Stretching vibration of O–H bond, 5: Bending vibrations of (HOH), 4, 6: Stretching vibration of CO_2, 7: Asymmetric stretching vibration (Si–O–Si), 8: Asymmetric stretching vibration (T–O–Si), 9: Symmetric stretching vibration of Al–OH, 10: Symmetric stretching vibration of CO_2, 11: Symmetric stretching vibration (Al–O–Si), 12: Symmetric stretching vibration (Si–O–Si), 13, 14: Bending vibration (Si–O–Si and O–Si–O)]

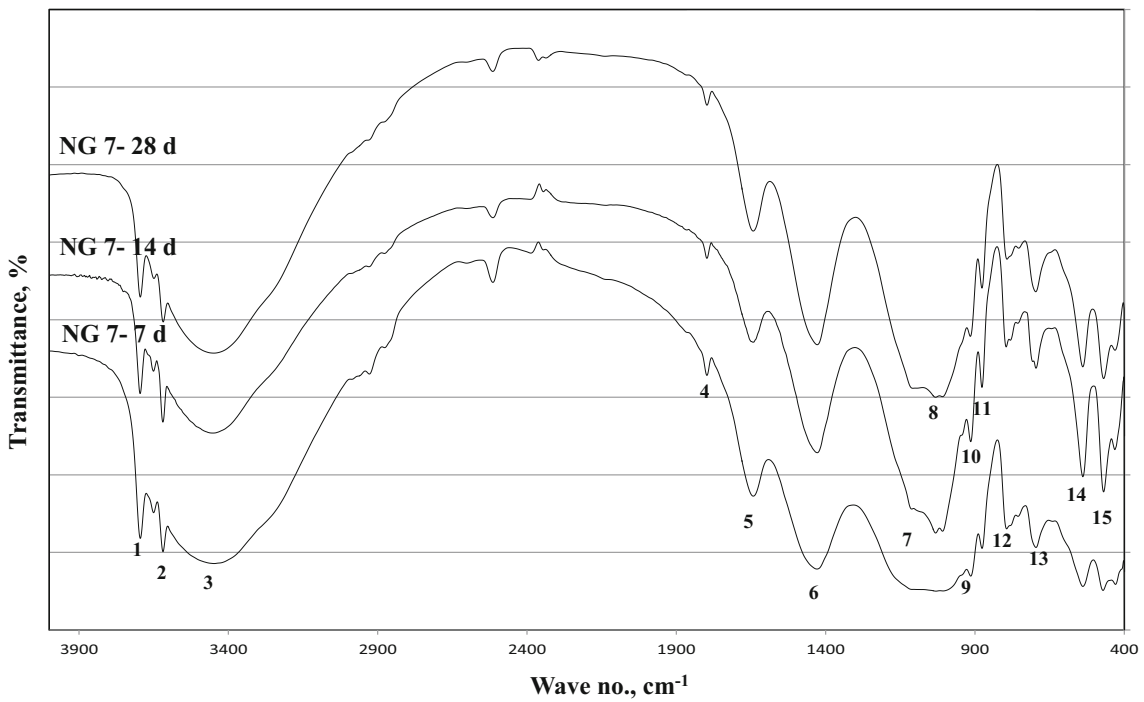

Fig. 4 FTIR spectra of alkali activated specimens enhanced with 7% nano-glass up to 28 days. [1: Stretching vibration of O–H bond, 2: Bending vibrations of (HOH), 3: Stretching vibration of CO_2, 4: Asymmetric stretching vibration (Si–O–Si), 5: Asymmetric stretching vibration (T–O–Si), 6, 7: Symmetric stretching vibration (Al–O–Si), 8, 9, 10: Symmetric stretching vibration (Si–O–Si), 11: Bending vibration (Si–O–Si and O–Si–O)]

There is a broadband for hydrating materials (CSH and CASH) as well as combined water within the matrix at 3455 cm^{-1}, this band seems to be increased with Ng as a result of interaction of free dissolved Ca species from slag precursor forming CSH that will offers additional binding materials as well as nucleation sites for geopolymer gel growth [39]. The spectra showed also a decrease in carbonate content at about 1430, 870 cm^{-1} with Ng as a result of increased geopolymer formation, while increase again with 9% Ng as a result of increased porosity that will be more prone to air entering and carbonation increase. It can be seen that intensity of the carbonate at about 1430–1450 cm^{-1} (ν C–O) subjected to splitting into two peaks which implies the distorted nature of CO_3 mineral [40, 41], as well as partial carbonation of C-S-H gel in air atmosphere.

XRD pattern of 28 days hardened alkali-activated mixes admixed with various ratios of Nano glass is shown in Fig. 5. The pattern illustrates a broad band in the region of 17° to 35° 2θ characterizing glassy phase of geopolymer constituent, this region exposed to increase with Nano glass addition up to 7% as a result of the increased enhancement by offering nucleation centers for geopolymer growth, however all mixes include kaolinite peaks in their pattern which decreases with Nano addition up to 7% as a results of enhanced dissolution of kaolinite by the added Nano materials as well as with the used alkalis leading to the increased amorphous content.

CSH phases increases with Ng up to 7%, while calcite decreases as a results of formation of homogenous matrix with low free alkalis available for carbonation. Whilst an increased Ng over this ratio results in formation of weak zone of agglomerated nanomaterials that are susceptible for carbonation as reflected on the increased intensity of calcite peaks as come in coincide with FTIR illustrations.

Studying effect of time on 7% Ng-based geopolymer mixes up to 28 days (Fig. 6) results in the intensity decrease of the kaolinite content, whilst the CSH phases increased with time as results of increased interaction of dissolved calcium and silica species forming the binding materials, this coexist with the increased broadness of glassy geopolymer band; reflecting an increased formation and growth of the geopolymer structures with time forming a dense structure.

The results of compressive strength for hardened mixes incorporating various Ng ratios and cured in 100% relative humidity at 40 °C up to 90 days are shown in Fig. 7. As a result of the ongoing dissolution and polymerization reaction as well as the ongoing growth of the geopolymer chains creating tightly bound structure, the results demonstrated an increase in strength for all mixes with hydration age.

There is an increased strength with Nano-glass up to 7%, and then subjected to gradual decrease with further Ng addition. This increase with Ng can be explained by increased geopolymer chain networks as results of increased nucleation sites for gel growth, in addition to the enhancement of Ng to the interaction of dissolved Ca supplied by the reacting precurors with some of the excess dissolved silicate present, forming additional strengthen binding materials (CSH, CASH) in addition to their role in providing nucleating agent for geopolymer formation and accumulation [42, 43], as illustrated clearly from XRD, FTIR. Decreasing strength up on using 9% Ng attributed to the agglomeration of the nanomaterial forming a weak zone for interaction of binding materials and so an increased porosity will be a barrier against their interaction.

3.2 Effect of Temperature on Nano-glass Powder Enhanced Geopolymer Composite

In comparison to the control mix, compressive strength for hardened alkali activated mixes comprising various ratios of nano-glass powder burned from 500 to 1000 °C for 2 h. With a heating rate of 5 °C/min is shown in Fig. 8. The results reveal an increase in compressive strength with up to 7% Ng- powder, followed by a drop in strength with more Nano glass powder. Furthermore, the strength of hardened pastes exposed to various temperatures grows up to 700 °C, and then decreases when fired at 800 °C, then increases when fired at 1000 °C.

Dehydroxylation of kaolinite materials forms metakaolin, which may enrich the matrix with excess amorphous materials, resulting in the creation of three-dimensional geopolymer that can survive high firing temperatures up to 700 °C. However, increasing the temperature to 800 °C causes strength degradation, which could be due to dehydration and dehydroxylation of the geopolymer structure. After decomposition of aluminosilicate gel free sodium, potassium, silicon, and aluminum, K-feldspars are formed, while sodium is in trace amounts and plays a minor role in feldspar formation.

The strength gain above 800 °C is primarily due to the appearance of metastable phases such as nephylene, gehlenite, and microcline in the geopolymer materials during firing, which resist thermal decomposition as evidenced by XRD, where the materials remained in the amorphous phase with reduced average pore size and significantly increased strength due to lower K-ion diffusion coefficient [44]. Additionally, the effect of the added Nano materials will add additional firing resistance to the fired matrix, enhancing the transition of calcite into marble. Marble is a metamorphic rock that forms when limestone is subjected to extreme heat and pressure. Where, Marble occurs under such conditions because the calcite in the limestone recrystallizes, resulting in a denser rock with about the same composition as the limestone [45].

The strength change factor (SCF) of fired Nano-enhanced geopolymer composites fired up to 1000 °C is shown in Fig. 9. SCF is a measure of how much strength is lost or gained when fired at different temperatures. Negative SCF

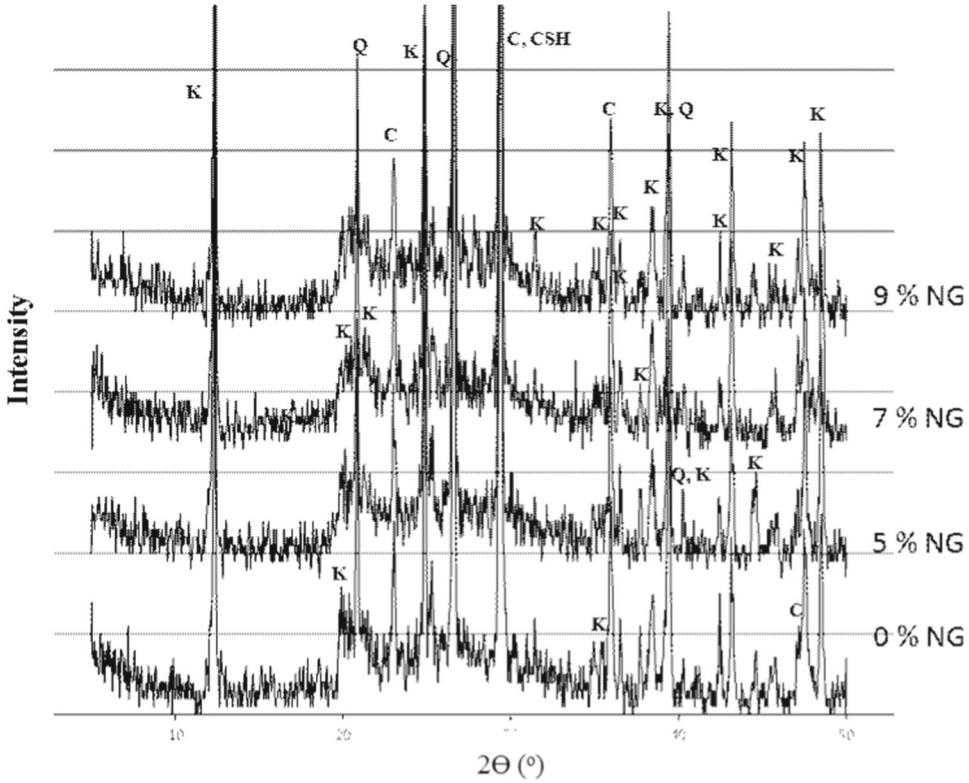

Fig. 5 XRD pattern of 28 days alkali activated specimens enhanced with various ratios of glass. [Q, quartz; K, kaolin; C, calcite; CSH, calcium silicate hydrate]

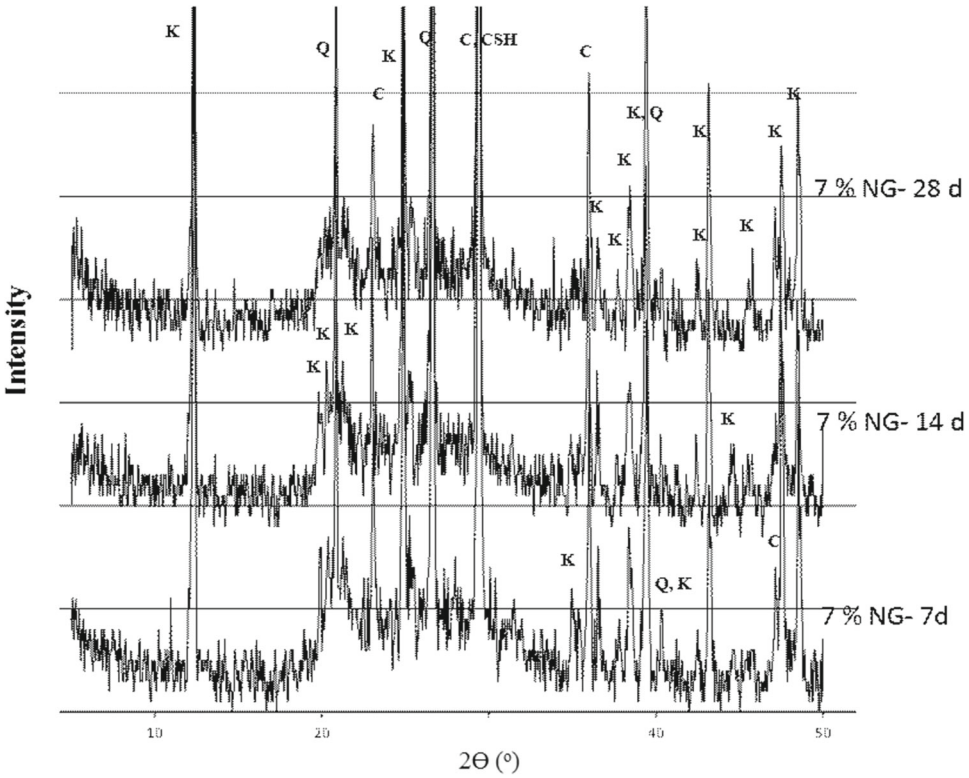

Fig. 6 XRD pattern of alkali activated specimens enhanced with 7% s nano-glass up to 28 days. [Q, quartz; K, kaolin; C, calcite; CSH, calcium silicate hydrate]

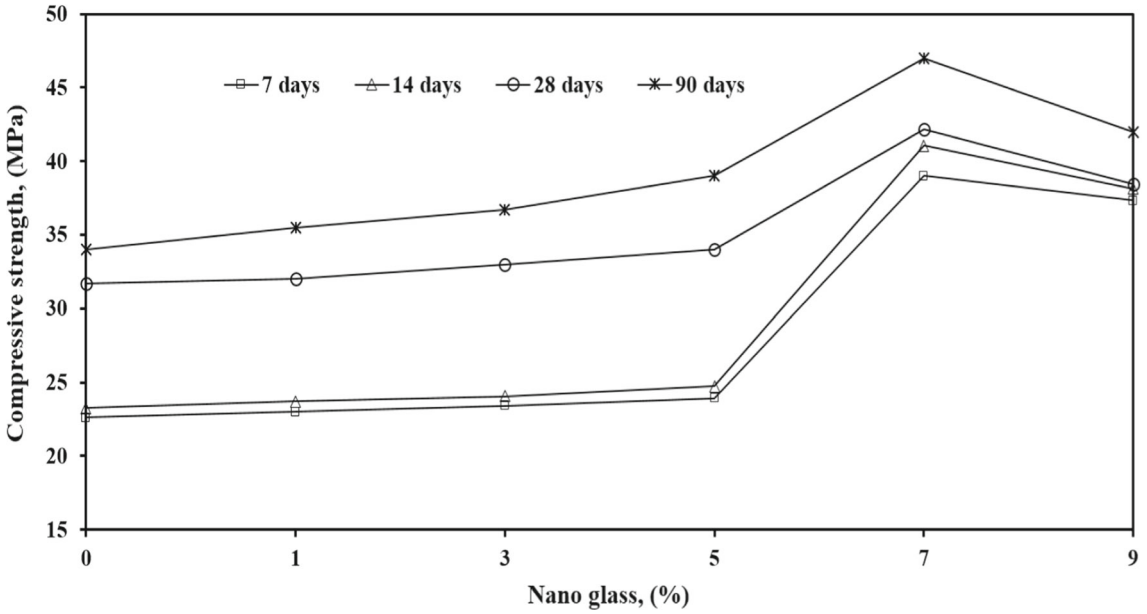

Fig. 7 Compressive strength of alkali activated specimens enhanced with various ratios of nano glass up to 90 days

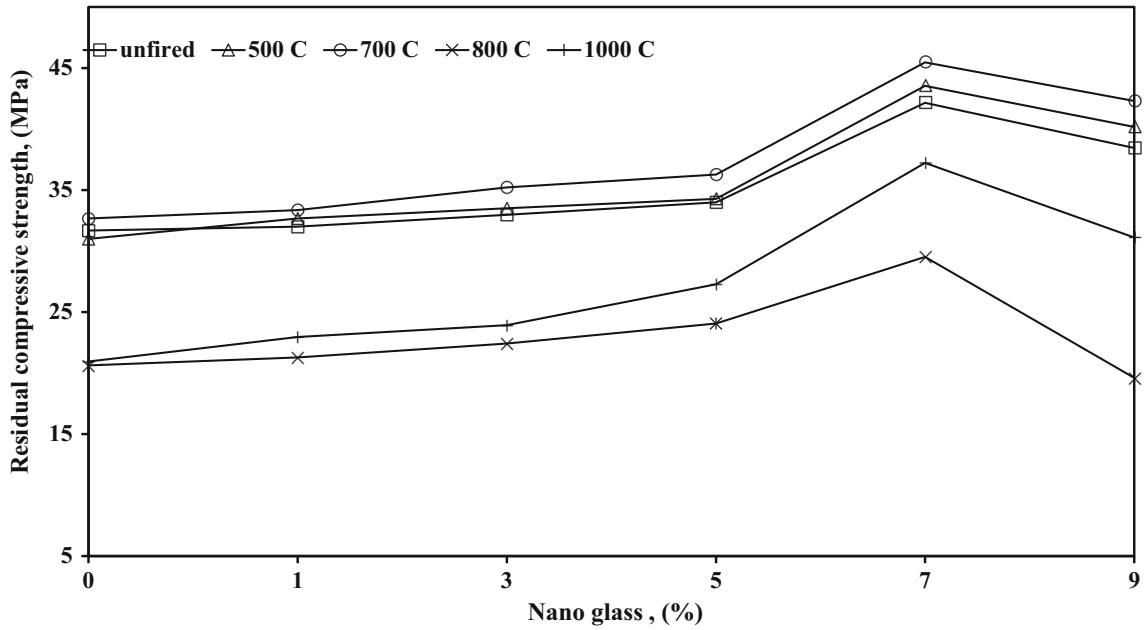

Fig. 8 Residual compressive strength of alkali activated specimens enhanced with various ratios of nano-glass and fired up to 1000 °C

values in concrete specimens without Nano-glass indicate an increase in compressive strength, which is most likely due to reaction product and crystallisation salt filling holes. Several researchers have also reported on this phenomenon [46].

Except for those fired at 500 and 700 °C and activated with Nano-glass powder, the figure depicts the increase in SCF with increasing temperature up to 1000 °C. The figure also shows that the SCF grows with higher temperatures, particularly between 800 and 1000 °C, but it exhibits lower values at 1000 °C than at 800 °C, as expected from the compressive strength pattern, which will be addressed in depth in the XRD section.

On the other hand, firing at 500 and 700 °C results in an increased strength as reflected in the negative value of SCF where the used kaolinite material transferred into metakaolin in addition to enhancing the effects of added Nano as well as the nucleation effect for geopolymer formation and accumulation, resulting in increased formation of geopolymer

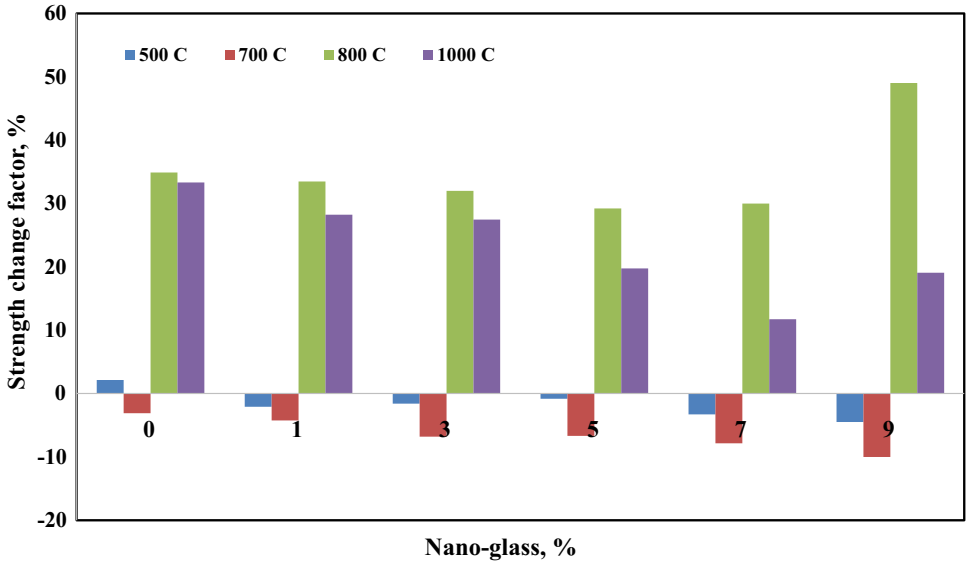

Fig. 9 Strength change factor of alkali activated specimens enhanced with various ratios of nano-glass and fired up to 1000 °C

chains. It's also worth noting that above 500 °C, composites lacking Nano-glass powder lose strength, confirming the activation effect of the Nano-materials.

Figure 10 shows the XRD pattern of a hardened alkali-activated geopolymer mix admixed with 7% Nano-glass powder and burned at various temperature. This region exposed to rise with increasing fire temperature up to 700 °C as a result of transformation of kaolinite elements into amorphous metakaolin, which has a beneficial impact on compressive strength qualities. Furthermore, the produced metakaolin can enrich the matrix with the amorphous aluminosilicate precursor, resulting in more geopolymer production.

When the temperature is raised to 800 °C, anorthite, albite, and microcline develop, all of which are feldspar phases with little amorphous character. When the temperature is raised to 1000 °C, metastable phases such as nephylene and gehlenite grow rapidly, resulting in the creation of a metamorphic phase of high-hardness calcite, which is marble with excellent thermal stability. The produced metastable phases may withstand high-temperature firing without deteriorating the composite. There is also evidence of crystalline feldspar phases such as microcline and anorthite contributing to the composition.

The endotherms at 55, 83, 106, 175, 467, 495, and 695–810 °C are represented by differential thermogravimetric curves for geopolymer mixes enhanced with 7% NG powder fired at different temperatures up to 1000 °C (Fig. 11), where the first and second are characteristic endotherms associated with the loss of freely bound water in aluminosilicate amorphous materials [46–48], the third associated with the dehydration of tightly bound in zeolite gismondine [49], the fourth associated with the dehydration of tightly bound water in a C-S-H gel [50], which is the main reaction product identified in GBFS-rich blended binders [51].

With firing to 500 °C, the intensity of the amorphous geopolymer decreases, as shown by an endothermic peak at around 55–84 °C merging to one endothermic peak. When the firing temperature is increased to 700 °C, the previous peak diminishes and the steady reduction continues. While increasing the temperature to 800 °C results in the formation of new feldspar phases, which may be responsible for strength degradation at 465 °C, which decrease and shift to 495 °C on firing to high temperatures as a result of transformation into another metastable phase (nephylene), despite the appearance of a new peak at 695 °C for marble that was exposed to intense growth on firing at 1000 °C [52].

Due to the high hardness of the aforementioned minerals that generated as metamorphic transformation of calcite, the later phase is accountable for the enhanced strength values for 1000 than for 800 °C. As previously discussed, XRD verified the earlier elucidations. Total weight loss for fired composites at 25, 500, 700, 800, and 1000 °C with 7% Nano-glass powder is 16.5, 10.8, 8.8, and 1.2%, respectively, as shown in Fig. 12. It can be seen that as the fire temperatures for geopolymer dehydration and calcination of unreacted metakaolin and calcite increase, the overall weight loss reduces, affecting the thermal stability of the produced composites.

A clear difference between samples was noted when visual evaluation was performed for fire hardened composites shot at various temperatures and incorporating varying Nano-glass ratios from 0 to 9%. All samples have a heat resistance of up to 700 °C, as evidenced by their mineralogical and bonding characteristics as determined by XRD and FTIR. This is related to kaolinite's dehydroxylation as well as nanoparticles' activation. Most samples show evident damage at 800 °C, with their colour shifting to a whiter hue as a

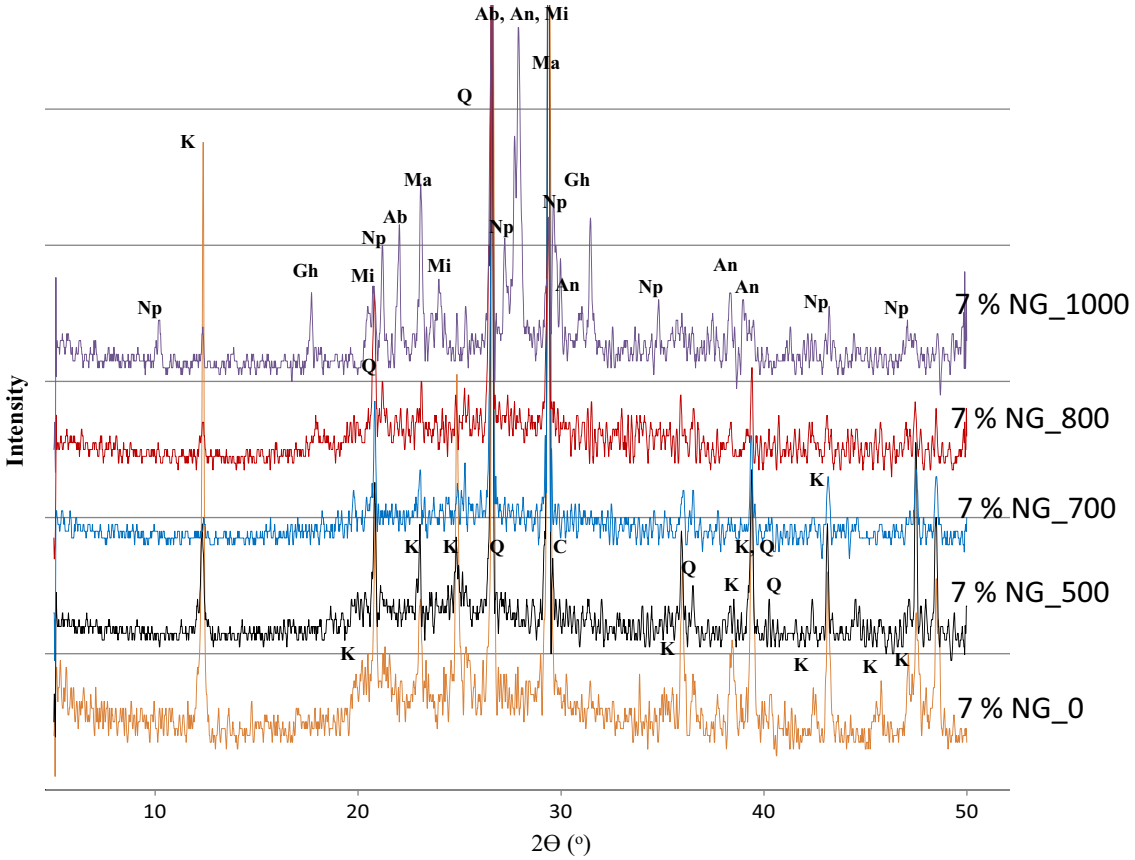

Fig. 10 XRD pattern of alkali activated specimens enhanced with 7% nano-glass fired up to 1000 °C [K, kaolin; Q, quartz; Np, nephylene; Gh, gehelenite; Ab, albite; Mi, microcline; An, anorthite, Ma, marble]

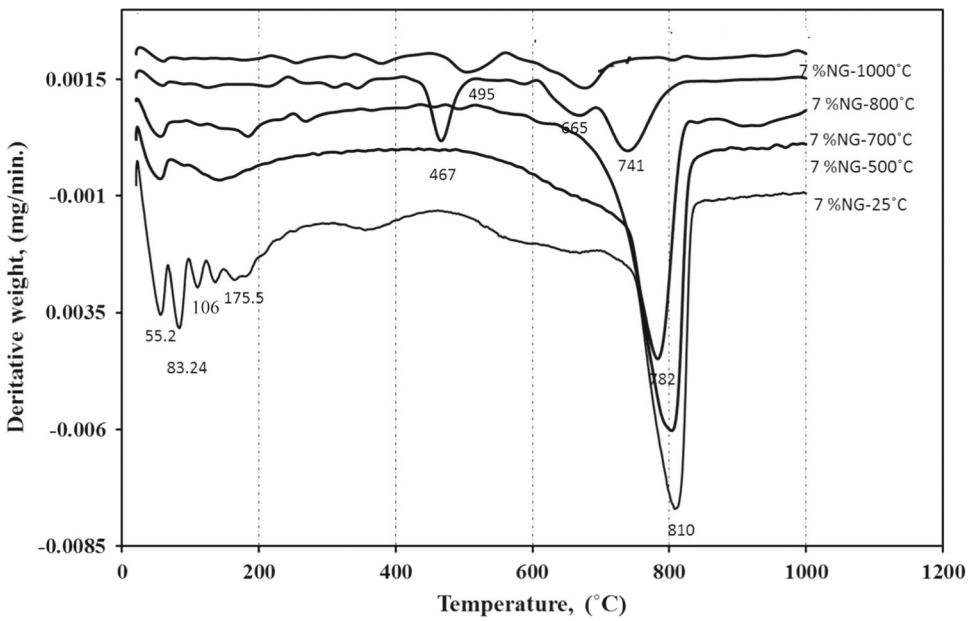

Fig. 11 Differential thermo-gravimetric pattern of alkali activated enhanced with 7% nano-glass fired up to 1000 °C

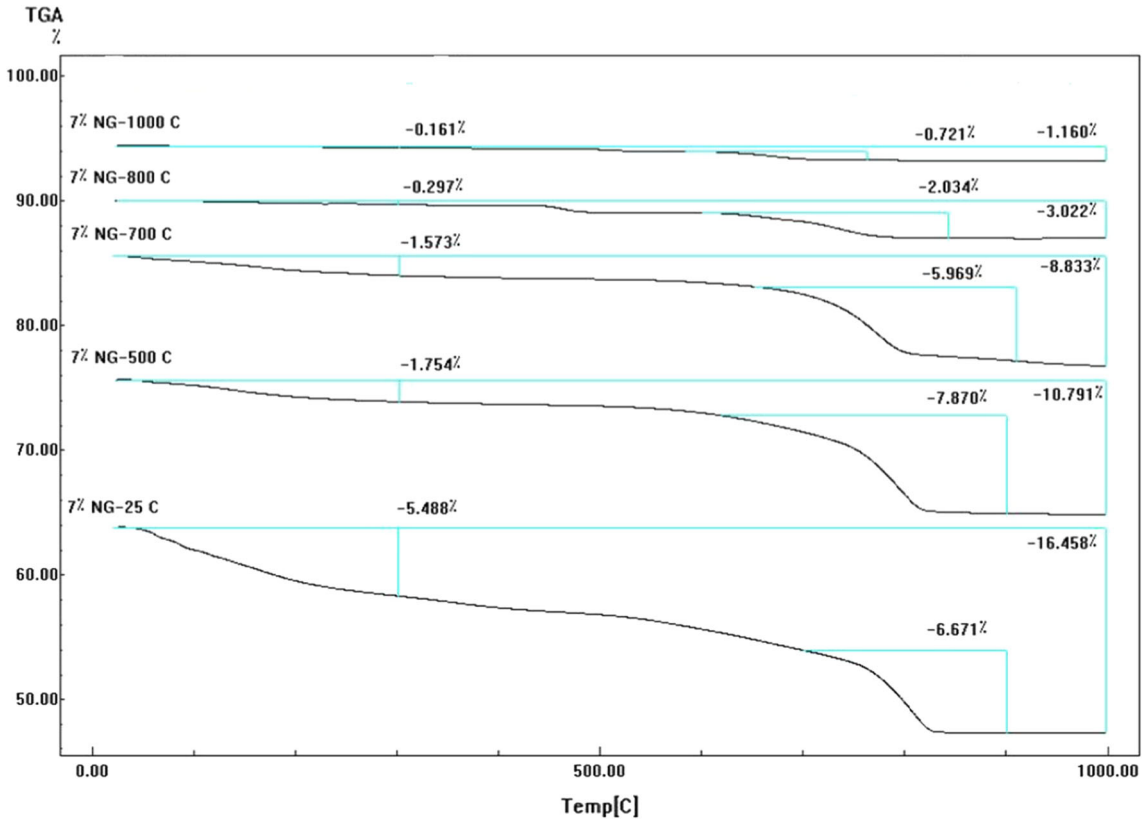

Fig. 12 TGA of alkali activated geopolymer specimens enhanced with 7% nano-glass fired up to 1000 °C

result of dehydration of CSH and binding phases within the matrix (Fig. 13).

On the other hand, most samples that are fired at 1000 °C encounter small microcrakcs with stable thermal cubes as a result of intense growth in metastable phases such as nephylene and gehlenite, as well as the formation of a metamorphic phase of high hardness calcite, which is marble with high thermal stability.

4 Conclusions

The main findings of this article are summarized below:

1. Addition of Nano-glass results in an enhancement in mechanical characteristics as well as mineralogical properties of the formed geopolymer composites.
2. The enhancement and modification of the hardened geopolymer specimens achieved when using Ng up to 7%, however further increase results in agglomeration and decrease in the efficiency of the added nanomaterials.
3. XRD and FTIR spectra confirm an intense amorphous geopolymer structure up on using 7% Ng.
4. The formed geopolymer mixes possess high mechanical properties that exceed 32 MPa after 28 days for control mix and increases with further NS up to 7%, giving a value of 42 MPa at 28 days and increased to 47 MPa at 3 months, which can be used in various building applications as infrastructure as well as fire resistant building materials.
5. Firing composites up to 1000 °C shows pronouncing stability up to 700 °C, while further increase in temperature results in formation of marble phase that can withstand against high temperatures.

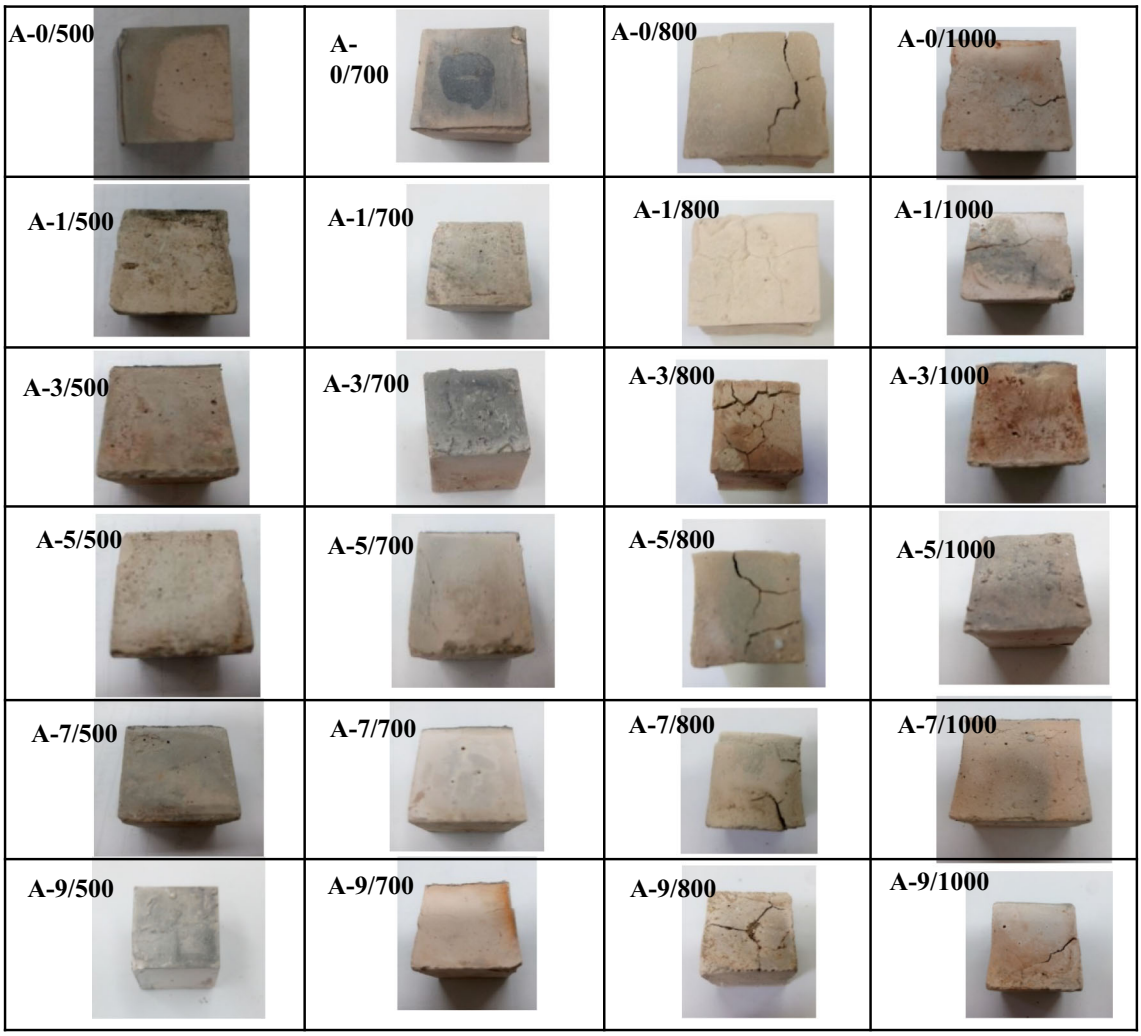

Fig. 13 Visual examination pattern of alkali activated specimens enhanced with various ratio of nano-glass fired up to 1000 °C

Author contributions HK: contribute for proposing the work of the paper, preparation of the materials, interpretation of the data, writing the manuscript as well as language editing. MG: contribute for proposing the work of the paper, preparation of the materials, interpretation of the data, writing the manuscript as well as language editing.

Funding Open access funding provided by The Science, Technology & Innovation Funding Authority (STDF) in cooperation with The Egyptian Knowledge Bank (EKB). There is no source of funding for the current paper.

Availability of data and material All data generated or analysed during this study are included in this published article [and its supplementary information files].

Declarations

Conflict of interest The authors declare that they have no known competing financial interests or personal relationships that could have appeared to influence the paper.

References

1. Balaguru, P.; Chong, K.: Nanotechnology and concrete research opportunities. In: Proceedings of the ACI Session on Nanotechnology of Concrete: Recent Developments and Future Perspectives, pp. 15–28 (2006)

2. Prince Arulraj, G.; Jemimah Carmichael, M.: Effect of nano fly ash on strength of concrete. Int. J. Civ. Eng. Struct. Eng. **2**(2), 475–482 (2011)
3. Khater, H.M.; El-Sabbagh, B.A.; Fanny, M.; Ezzat, M.; Lottfy, M.: Effect of nano-silica on alkali activated water-cooled slag geopolymer. ARPN J. Sci. Technol. **2**(3), 170–176 (2012)
4. Kuo, W.-Y.; Huang, J.-S.; Lin, C.-H.: Effects of organo-modified montmorillonite on strengths and permeability of cement mortars. Cem. Concr. Res. **36**, 886–895 (2006)
5. Li, H.; Xiao, H.; Ou, J.: A study on the mechanical and pressure sensitive properties of cement mortar with nano phase materials. Cem. Concr. Res. **34**, 435–438 (2004)
6. Möschner, G.; Lothenbach, B.; Winnefeld, F.; Ulrich, A.; Figi, R.; Kretzschmar, R.: Solid solution between Al-ettringite and Fe-ettringite ($Ca_6[Al_{1-x}Fe_x(OH)_6]_2(SO_4)_3{\cdot}26H_2O$). Cem. Concr. Res. **39**(6), 482–489 (2009)
7. Patel, V.K.; Chauhan, S.; Katiyar, J.K.: Physico-mechanical and wear properties of novel sustainable sour-weed fiber reinforced polyester composites. Mater. Res. Express **5**(4), 045310 (2018)
8. Khater, H.M.: Effect of nano silica on microstructure formation of low cost geopolymer binder. J. Nanocompos. **2**(2), 84–97 (2016). https://doi.org/10.1080/20550324.2016.1203515
9. Khater, H.M.; Abd el Gawwad, H.A.: Synthesis and characterization of MK/Slag geopolymer composites enhanced by various ratios of nano kaolin, építôanyag. J. Silic. Based Compos. Mater. **69**(2), 40–48 (2017). https://doi.org/10.14382/epitoanyag-jsbcm.2017.8
10. Buffat, P.; Burrel, J.-P.: Size effect on the melting temperature of gold particles. Phys. Rev. A. **13**(6), 2287 (1976)
11. Negi, A.S.; Katiyar, J.K.; Kumar, S.; Kumar, N.; Patel, V.K.: Physicomechanical and abrasive wear properties of hemp/Kevlar/carbon reinforced hybrid epoxy composites. Mater. Res. Express **6**(11), 115304 (2019)
12. Hui, L.; Zhang, M.H., et al.: Flexural fatigue performance of concrete containing nano- particles for pavement. Int. J. Fatigue **29**, 1292–1301 (2007)
13. Wang, J.; Wang, L.: Advances in the applied research of nanomaterial in concrete. Concrete **11**, 18–21 (2004)
14. Cyr, M.; Lawrence, P., et al.: Efficiency of mineral admixtures in mortars: quantification of the physical and chemical effects of fine admixtures in relation with compressive strength. Cem. Concr. Res. **36**, 264–277 (2006)
15. Li, H.; Xiao, H.-G., et al.: Microstructure of cement mortar with nano-particles. Compos. Part B Eng. **35**, 185–189 (2004)
16. Dolado, J.S.; Campillo, I.; Erkizia, E.; Ibanez, J.A.; Porro, A.; Guerrero, A.; Goñi, S.: Effect of nanosilica additions on belite cement pastes held in sulfate solutions. J. Am. Ceram. Soc. **90**(12), 3973–3976 (2007)
17. Li, G.: Properties of high-volume fly ash concrete incorporating nano-SiO_2. Cem. Concr. Res. **34**, 1043–1049 (2004)
18. Gaitero, J.J.; Campillo, I.; Mondal, P.; Shah, S.P.: Small changes can make a great difference. In: 1st International Conference in North America on Nanotechnology in Cement and Concrete, Irvine, CA 5–7 May 2010. NANO10-0019 (2010).
19. Seo, J.H.; Kim, D.U.; Nam, J.S.; Hong, S.H.; Sohn, S.B.; Song, S.M.: Radio frequency thermal plasma treatment for size reduction and spheroidization of glass powders used in ceramic electronic devices. J. Am. Ceram. **90**(6), 1717–1721 (2007)
20. Turaka, S.; Reddy, K.V.K.; Sahu, R.K.; Katiyar, J.K.: Mechanical properties of MWCNTs and graphene nanoparticles modified glass fibre-reinforced polymer nanocomposite. Bull. Mater. Sci. **44**(3), 1–14 (2021)
21. Khater, H.M.: Calcium effect on geopolymerization of alumino silicate wastes. J. Mater. Civ. Eng. **24**(1), 92–101 (2012)
22. Khater, H.M.: Effect of silica fume on the characterization of the geopolymer materials. Int. J. Adv. Struct. Eng. **5**(12), 1–10 (2013)
23. Kakali, G.; Perraki, T.; Tsivilis, S.; Badogiannis, E.: Thermal treatment of kaolin: the effect of mineralogy on the pozzolanic activity. Appl. Clay Sci. **20**, 73–80 (2001)
24. Wenying, G.; Guolin, W.; Jianda, W.; Ziyun, W.; Suhong, Y.: Preparation and performance of geopolymers. J. Wuhan Univ. Technol. Mater. Sci. Ed. **23**(3), 285–430 (2008)
25. Collins, F.; Lambert, F.; Duan, W.H.: The influence of admixtures on the dispersion, workability, and strength of carbon nanotube OPC paste mixtures. Cem. Concr. Compos. **34**(9), 1067–1074 (2012)
26. Senff, L.; Hotza, D.; Repette, W.L.; Ferreira, V.M.; Labrincha, J.A.: Effect of nanosilica and microsilica on microstructure and hardened properties of cement pastes and mortars. Adv. Appl. Ceram. **109**(2), 104–110 (2010)
27. ASTM C109M-12. Standard Test Method for Compressive Strength of Hydraulic Cement Mortars (2012)
28. Saikia, N.; Usami, A.; Kato, S.; Kojima, T.: Hydration behavior of ecocement in presence of metakaolin. Resour. Progress. J. **51**(1), 35–41 (2004)
29. Khater, H.M.: Influence of metakaolin on resistivity of cement mortar to magnesium chloride solution. Ceram. Silikáty J. **54**(4), 325–333 (2010)
30. Egyptian Standards. Concrete building units used in non-load and load bearing walls, 1292. Egyptian Organization for Standardization, Cairo (1992)
31. Ugheoke, B.I.; Onche, E.O.; Namessan, O.N.; Asikpo, G.A.: Property optimization of kaolin-rice husk insulating fire-bricks. Leonardo Electron. J. Pract. Technol. **9**, 167–178 (2006)
32. Ganjian, E.; Pouya, H.: Effect of magnesium and sulfate ions on durability of silica fume blended mixes exposed to the seawater tidal zone. Cem. Concr. Res. **35**, 1332–1343 (2005)
33. Bernal, S.; De Gutierrez, R.; Delvasto, S.; Rodriguez, E.: Performance of an alkali-activated slag concrete reinforced with steel fibers. Constr. Build. Mater. **24**(2), 208–214 (2010)
34. de Vargas, A.S.; Dal Molin, D.C.; Masuero, Â.B.; Vilela, A.C.; Castro-Gomes, J.; de Gutierrez, R.M.: Strength development of alkali-activated fly ash produced with combined NAOH and $CA(OH)_2$ activators. Cem. Concr. Compos. **53**, 341–349 (2014)
35. Panias, D.; Giannopoulou, I.P.; Perraki, T.: Effect of synthesis parameters on the mechanical properties of fly ash-based geopolymers. Colloids Surf. A Physicochem. Eng. Asp. **301**, 246–254 (2007)
36. Bakharev, T.: Durability of geopolymer materials in sodium and magnesium sulfate solutions. Cem. Concr. Res. **35**, 1233–1246 (2005)
37. Palomo, A.; Grutzeck, M.W.; Blanco, M.T.: Alkali-activated fly ashes: cement for future. Cem. Concr. Res. **29**, 1323–1329 (1999)
38. Rees, C.A.; Provis, J.L.; Lukey, G.C.; van Deventer, J.S.J.: The mechanism of geopolymer gel formation investigated through seeded nucleation. Colloids Surf. A Physicochem. Eng. Asp. **318**, 97–105 (2008)
39. Temuujin, J.; Van Riessen, A.; Williams, R.: Influence of calcium compounds on the mechanical properties of fly ash geopolymer pastes. J. Hazard. Mater. J. Hazard. Mater. **167**(1–3), 82–88 (2009)
40. Kalinkin, A.M.; Politov, A.A.; Boldyrev, V.V.; Kalinkina, E.V.; Makarov, V.N.; Kalinnikov, V.T.: Study of mechanical activation of diopside in a CO_2 atmosphere. J. Mater. Syn. Proc. **38**, 163–167 (2002)
41. Kalinkin, A.M.; Kalinkina, E.V.; Politov, A.A.; Makarov, V.N.; Boldyrev, V.V.: Mechanochemical interaction of Ca silicate and aluminosilicate minerals with carbon dioxide. J. Mater. Sci. **39**, 5393–5398 (2004)
42. Van Deventer, J.S.J.; Provis, J.L.; Duxson, P.; Luckey, G.C.: Reaction mechanisms in the geopolymeric conversion of inorganic waste to useful products. J. Hazard. Mater. **A139**, 506–513 (2007)

43. Lee, W.K.W.; Van Deventer, J.S.J.: The effect of ionic contaminants on the early age properties of alkali-activated fly ash based cements. Cem. Concr. Res. **32**, 577–584 (2002)
44. Khater, H.M.; Zedane, S.R.: Geopolymerization of industrial by-products and study of their stability upon firing treatment. Int. J. Eng. Technol. **2**(2), 308–316 (2012)
45. Gomes, S.; Petit, E.; Frezet, L.; Thirouard, R.; Taviot-Gueho, R.; Gharzouni, A.; Rossignol, S.; Renaudin, G.: Temperature stability of a pure metakaolin based K-geopolymer: part 1. Variations in the amorphous mineral network. J. Am. Ceram. Soc. **103**(10), 5813–5824 (2020)
46. Al-Amoudi, O.S.B.; Rasheeduzzafar, T.; Maslehudin, M.; Abduljauwad, S.N.: Influence of chloride ions on sulfate deterioration in plain and blended cements. Mag. Concr. Res. **46**, 113–123 (1994)
47. Weitzel, B.; Hansen, M.R.; Kowald, T.L.; Müller, T.; Spiess, H.W.; Trettin, H.F.R.: Influence of multiwalled carbon nanotubes on the microstructure of CSH-phases. In: Proceeding of 13th Congress on the Chemistry of Cement, Madrid, Spain, pp. 3–8 (2011)
48. Alarcon-Ruiz, L.; Platret, G.; Massieu, E.; Ehrlacher, A.: The use of thermal analysis in assessing the effect of temperature on a cement paste. Cem. Concr. Res. **35**(3), 609–613 (2005)
49. Buchwald, A.; Tatarin, R.; Stephan, D.: Reaction progress of alkaline-activated metakaolin-ground granulated blast furnace slag blends. J. Mater. Sci. **44**, 5609–5617 (2009)
50. Bernal, S.A.; Rodríguez, E.D.; Mejía de Gutierrez, R.; Gordillo, M.; Provis, J.L.: Mechanical and thermal characterisation of geopolymers based on silicate-activated metakaolin/slag blends. J. Sci. Mater. **46**, 5477 (2011). https://doi.org/10.1007/s10853-011-5490-z
51. Bernal, S.A.; Provis, J.L.; Rose, V.; Mejía de Gutiérrez, R.: Evolution of binder structure in sodium silicate-activated lag metakaolin blends. Cem. Concr. Compos. **33**(1), 46–54 (2011)
52. Engelhardt, G.; Felsche, J.; Sieger, P.: The hydrosodalite system Na6+x[SiAlO4]6(OH)x.nH2O: formation, phase composition, and de- and rehydration studied by 1H, 23Na, and 29Si MAS-NMR spectroscopy in tandem with thermal analysis, X-ray diffraction, and IR spectroscopy. J. Am. Chem. Soc. **114**, 1173–82 (1992)